Aggregation of Concentrated Polymer Latex in Stirred Vessels

Andrea Vaccaro, Ján Šefčík, Hua Wu, and Massimo Morbidelli
Swiss Federal Institute of Technology Zurich, Institut für Chemie- und Bioingenieurwissenschaften, ETH Hönggerberg/HCI, CH-8093 Zürich, Switzerland

Josselin Bobet and Christophe Fringant
Solvin France S.A., F-39501 Tavaux Cedex, France

DOI 10.1002/aic.10843
Published online May 3, 2006 in Wiley InterScience (www.interscience.wiley.com).

An assessment of the relative magnitude of the timescales of mixing and aggregation of fully destabilized polymeric latices in stirred vessels is presented. It is demonstrated that, in industrially relevant conditions (that is, volume fractions above 10% and primary aggregate sizes below 200 nm), latices aggregate and possibly gel before complete mixing is achieved. By means of focused beam reflectance measurements, we measure on-line and in situ *the size of aggregates obtained aggregating a PVDC latex at salt concentrations above the critical coagulation concentration in a stirred vessel operated in semibatch. Several experimental runs are conducted and averages of the aggregate size distribution, that is, volume and number averages, are measured at various values of the feed flowrate, feed solid volume fraction, stirring speed and final volume fraction in the vessel. It is found that at high feeding volume fractions aggregates instantaneously aggregate and gel on entering the vessel. Resulting aggregates are then broken down to volume weighted average sizes falling in the range between 100 and 400 microns at steady state. The experimental results are interpreted in terms of a competition between the aggregation/gelation process and mixing. In particular, by evaluating the relevant characteristic times, it is found that the process is dominated by the competition between mesomixing at the location, where the latex enters the vessel and the aggregation/gelation process. Scanning electron micrographs of dry samples obtained after thermal treatment show aggregate morphologies which further support the above interpretation.* © 2006 American Institute of Chemical Engineers *AIChE J,* 52: 2742–2756, 2006
Keywords: aggregation, gelation, polymer latex, coagulator, mesomixing, micromixing

Introduction

A sizeable amount of polymeric materials are produced via emulsion polymerization due to its inherent thermal control, high-productivity even for high-molecular weights and moderate viscosity increases.[1,2] Another advantage of emulsion polymerization resides in the colloidal nature of the final product. Due to its physical properties the final latex can be used "as such" in many applications, such as for example paints, coating and finishes. On the other hand, when the application requires the polymeric material in powder form, a process for separating the polymer from water has to be set up.

At colloidal sizes Brownian motion effectively suppresses the tendency of the polymer particles to sediment due to their density difference with the suspending medium. Consequently, a stable latex, in which polymer particles effectively repel each

Correspondence concerning this article should be addressed to M. Morbidelli at morbidelli@chem.ethz.ch.

other, shows a negligible tendency to phase separate. When the stabilization mechanism is removed, Brownian motion and macroscopic velocity gradient can cause polymer particles to collide and stick together due to van der Waals attraction, thus, leading to aggregates of larger size. Such aggregation process[3] eventually brings about sedimentation due to the system's loss of colloidal character, thus, leading to phase separation. Accordingly, aggregation appears to be a viable route in the setup of an industrial process for separating the solid phase from water in polymeric latices.

Several methods for imparting colloidal stability exist. One of the most commonly adopted relies on electrostatic repulsion forces. In this stabilization mechanism an amphiphilic ionic species is added to the dispersion so that, by adsorbing at the polymer particle surface, a surface charge is developed. As a result a repulsive interparticle Coulomb force arises, providing stabilization by preventing particle collisions. When a strong electrolyte is added to an electrostatically stabilized latex, the ions effectively screen the existing surface charge, colloidal stability is lost, and, consequently, particles aggregate. The aggregation rate strongly increases upon increasing electrolyte concentration. Above the critical coagulation concentration (CCC) repulsion forces are completely screened, and the aggregation rate reaches a constant value where the process becomes diffusion limited. Accordingly, a typical industrial process for separating the polymer phase from water in an electrostatically stabilized latex is based on mixing a salt solution with the latex in an agitated vessel operated in batch or continuous mode. It is commonly chosen to work in fully destabilized conditions, that is, at salt concentrations above CCC, in order to avoid the aforementioned strong dependency of the aggregation rate upon salt concentration, consequently favoring the productivity, and the robustness of the process. In these conditions the aggregation process becomes very fast, thus, competing with the mixing process typical of stirred vessels, and leading to gels even in the presence of substantial breakage.

The complex interplay among these processes is not investigated in the literature covering salt induced aggregation of electrostatically stabilized latices in agitated vessels,[4–12] where the aggregation process is significantly slowed down by operating at extremely low particle volume fractions. In addition, the particle size of the latices used in the aggregation experiments is normally above 1 micron, which is far bigger than the particle sizes in typical industrial latices, which are of the order of hundred nanometers.

In this work we address these issues by performing suitable experiments in a stirred vessel with fully destabilized latices of a small particle size in concentrated conditions, which are the conditions typical of industrial applications. By monitoring on-line and *in situ* the time evolution of the size distribution of the polymer aggregate dispersion, we can derive information about the competition between aggregation, breakage and the mixing processes. These are relevant aspects in the design of a coagulation unit since the aggregate size distribution is one of the main characteristics in determining the value of the final polymer powder. The importance of these considerations can be better appreciated when considering that, in a typical coagulation unit, aggregates of average size of the order of 100–500 μm are produced starting from latices of primary particles whose size is of the order of 100 nm. This corresponds to a scale-up factor of 3 to 4 orders of magnitude.

Theoretical Aspects

Aggregation and breakage in stirred vessels

Aggregation and breakage of colloidal aggregates in ideal stirred vessels can be modeled by means of the following population balance for the k-fold aggregate (that is, an aggregate containing k primary particles) known as the Smoluchowski coagulation equation[13]

$$\frac{dN_k}{dt} = \frac{1}{2}\sum_{i+j=k} K_{ij}N_i(t)\,N_j(t) - N_k(t)\sum_i K_{ki}N_i(t) + \\ - \Gamma_k N_k(t) + \sum_i \Gamma_i \Delta_{ik} N_i(t) \quad (1)$$

where $N_i(t)$, $N_j(t)$ and $N_k(t)$ are the number concentrations of the i-fold, j-fold and k-fold aggregate at time t, respectively. The first two terms on the righthand side represent the effect of aggregation and the last two represent the effect of breakage. The matrix of second order aggregation rate constants K_{ij}, usually referred to as the aggregation kernel, reflects the physics of the aggregation process. The breakage rate is described using a first-order kinetic model[8] where Γ_k is the corresponding rate constant for a aggregate of mass k, which generally depends on aggregate size and turbulent intensity, while Δ_{ik} represents the fraction of fragments of mass k originating from the disruption of a aggregate of mass i, and is usually referred to as the daughter distribution function. In fully destabilized conditions, as those considered here, it is reasonable to assume[14] the aggregation kernel to be expressed by the sum of two contributions, K_{ij}^{Brown} and K_{ij}^{Turb}, due to Brownian motion and turbulent flow, respectively. For collisions of aggregates of sizes R_i and R_j their expressions read[13,15]

$$K_{ij}^{\text{Brown}} = 4\pi(R_i + R_j)(D_i + D_j) \quad (2)$$

$$K_{ij}^{\text{Turb}} = \sqrt{\frac{8}{15}\pi}\sqrt{\frac{\varepsilon}{\nu}}(R_i + R_j)^3 \quad (3)$$

where ε is the rate of turbulent energy dissipation, ν is the suspending medium kinematic viscosity, and D_i and D_j are the aggregates diffusion coefficients. The diffusion coefficient of an i-fold aggregate can be expressed by means of the Stokes-Einstein relation as follows

$$D_i = \frac{k_B T}{6\pi\mu\beta R_i} \quad (4)$$

where k_B is the Boltzmann constant, β is a constant of order one accounting for the shape of the aggregate, and μ is the suspending medium viscosity. In order to close the model 1 to 4 an expression relating the aggregate size to its mass, based on some assumption about its structure, has to be provided. In the case of pure Brownian aggregation, it has been shown[16] that such a relationship for an aggregate made up of i particles is given by

$$i = k_0\left(\frac{R_i}{a}\right)^{d_f} \tag{5}$$

where $d_f \simeq 1.8$ is the fractal dimension, k_0 is a constant of order one, and a is the primary particle radius. This result is known as fractal scaling. Since the scaling indicates that the aggregate density decreases with size, at some point of their growth space will be filled and gelation occurs,[17] thus, resulting in one single aggregate spanning the whole system.

In the case of semibatch operation where a salt solution above CCC, and a stable polymeric latex with particle number concentration N_k^F are fed into the system at volumetric feed rates Q_S and Q_L, respectively, Eq. 1 is modified as follows

$$\frac{dN_k}{dt} + \frac{N_k(t)}{V(t)}\frac{dV}{dt} = \frac{Q_L}{V(t)}N_k^F + \frac{1}{2}\sum_{i+j=k} K_{ij}N_i(t)N_j(t) + \\ - N_k(t)\sum_i K_{ki}N_i(t) - \Gamma_k N_k(t) + \sum_i \Gamma_i \Delta_{ik} N_i(t) \tag{6}$$

where the total volume of the system, $V(t)$, is a function of time and can be obtained by writing a suitable mass balance on the whole system. It is to be noted that, in writing the equations above, we have tacitly assumed that aggregation and breakage are slow compared to mixing, and that the stirred vessel can be regarded as a uniform system with respect not only to composition, but also to the energy dissipation rate.

Time Scales of Mixing and Aggregation

Let us consider a stream of stable latex at solid volume fraction ϕ_F entering an agitated vessel containing a salt solution at a concentration well above CCC. As the latex volume enters the system, it is stretched and folded by the turbulent motion of the salt solution. At the same time, salt molecules diffuse into it through its boundaries. As time elapses, the stretching and folding mechanism will impart a lamellar structure to the volume itself,[18] thus, increasing its surface area and decreasing its characteristic length scale. This process lasts until a length scale is attained where salt molecular diffusion becomes effective and the mixing at smaller scales is complete. Let us call the characteristic time of this process τ_M. It should be noticed that τ_M refers to the salt, while the polymer particles, whose diffusion coefficient is smaller by at least two orders of magnitude, certainly exhibit a larger mixing time.

In this frame we can consider that, as the local salt concentration in the latex volumes (whose disruption is controlled by mixing) increases, colloidal stability is lost and aggregation becomes significant. Due to the strong sensitivity of the aggregation rate to the salt concentration, it can be safely assumed that aggregation is very slow until the CCC is reached. However, at the CCC and above, the characteristic time of aggregation τ_A can be either smaller or larger than τ_M. In the case $\tau_A \ll \tau_M$, the aggregation process would take place before mixing is complete. This has the important consequence that, since salt molecules diffuse at a far larger rate into the latex volume than the polymer particles into salt volumes, aggregation mainly occurs at volume fractions very near the feeding volume fraction ϕ_F. This tends to be substantially large and therefore can easily lead to gelation. As a consequence, at very high feed solid volume fractions gelation can freeze in latex volumes into gel aggregates whose size is dictated by the extent of the reduction of the initial latex volume caused by turbulent mixing which was reached at the time where gelation occurred. On the other hand, if $\tau_A \gg \tau_M$ aggregation occurs uniformly in the entire vessel, which means also very low aggregate concentrations, thus, making the gelation process more unlikely. It is clear that the final powder obtained in the two cases might end up being very different in terms of both particle structure and aggregate size distribution (ASD).

In order to assess the likelihood of the above scenario let us evaluate the aggregation, gelation and mixing timescales based on simple models of aggregation and turbulent mixing available in the literature. In the above conditions the initial aggregation rate corresponds to the aggregation of primary particles whose aggregation rate constant K_{11} can be derived from Eqs. 2 and 3 as follows

$$K_{11} = \frac{8k_BT}{3\mu} + 8\sqrt{\frac{8}{15}\pi}\sqrt{\frac{\varepsilon}{\nu}}a^3 \tag{7}$$

Considering that aggregation follows a second-order kinetics in particle number concentration N_F, the corresponding aggregation characteristic time τ_A is given by

$$\tau_A = \frac{1}{K_{11}N_F} = \left(\frac{2k_BT}{\pi\mu a^3}\phi_F + \frac{6}{\pi}\sqrt{\frac{8}{15}\pi}\sqrt{\frac{\varepsilon}{\nu}}\phi_F\right)^{-1} \tag{8}$$

where the particle number concentration has been expressed in terms of the solid volume fraction as $N_F = 3\phi_F/(4\pi a^3)$, and it was assumed, according to the earlier discussion, that aggregation at the very beginning takes place at the particle concentration value in the feed stream. On the other hand, if the time required by the turbulent flow to reduce the characteristic lengthscale of the feed to the Kolmogorov microscale is very short, τ_M is on the order of the smallest time scale of a turbulent flow, namely the Kolmogorov time scale τ_η[19]

$$\tau_M \simeq 17\tau_\eta = 17\sqrt{\frac{\nu}{\varepsilon}} \tag{9}$$

In order to evaluate the relative magnitude of the two characteristic times, the contour plot of the logarithm of the ratio of the characteristic time of mixing τ_M to the characteristic time of aggregation τ_A, τ_M/τ_A is shown in Figure 1. The range of particle sizes and volume fractions typically explored in the literature under shear aggregation conditions ($10^{-5} < \phi < 10^{-3}$ and 0.8 μm $< a <$ 2 μm),[4–12] is represented by the crosshatched area. It can be seen that these conditions correspond to $\tau_M/\tau_A \simeq 10^{-2}$, so that it is safe to assume that aggregation occurs on a timescale long enough to avoid mixing effects on the aggregation kinetics. On the other hand, if we consider conditions typical for industrial applications (hatched area in Figure 1), that is, small particle radii (for example, in the case of polymeric latices, in the range between 40 and 150 nm), and high-volume fractions (say larger than 0.1), the situation radically changes and the aggregation is mixing-controlled. In these conditions, the aggregation time scale is at

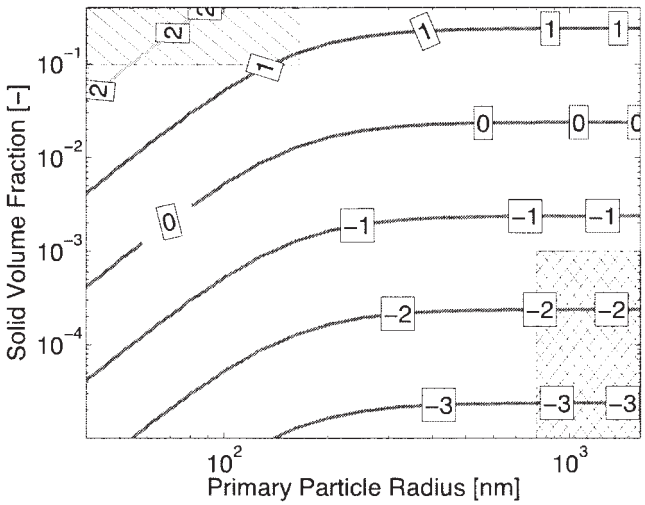

Figure 1. Contour plot of the logarithm of the ratio τ_M/τ_A between the characteristic time of micromixing and the characteristic time of aggregation as a function of primary particle radius and solid volume fraction in the latex.

Labels represent the value of the logarithm corresponding to the isoline. Values of the parameters used for the computations: $T = 298$ K, $\varepsilon = 0.1$ W/kg, $\mu = 8.91 \cdot 10^{-4}$ Pa sec, $\nu = 8.91 \cdot 10^{-7}$ m^2/sec.

least one order of magnitude smaller than that of mixing. This arises because smaller particles have higher diffusion coefficients, thus, enhancing aggregation, and higher volume fractions imply higher particle number concentrations that in turn lead to smaller aggregation characteristic times, since aggregation follows second order kinetics.

Let us now bring into this frame also the gelation process. Since for small particles turbulent shear aggregation is negligible compared to Brownian aggregation, we use a simple model of Brownian aggregation to estimate the characteristic timescale of gelation τ_G. In static conditions the Smoluchowski coagulation equation reads

$$\frac{dN_k}{dt} = \frac{1}{2}\sum_{i+j=k} K_{ij}N_i(t)\,N_j(t) - N_k(t)\sum_i K_{ki}N_i(t) \qquad (10)$$

where the aggregation kernel can be expressed using Eq. 2 and Eq. 4 as follows

$$K_{ij} = K_{ij}^{\text{Brown}} = \frac{2k_BT}{3\mu}(R_i + R_j)\left(\frac{1}{R_i} + \frac{1}{R_j}\right)$$

In Brownian DLCA aggregation, as time elapses, the mass distribution remains fairly monodisperse, consequently, as a first approximation it can be described using the constant kernel $K_{ij} = 8k_BT/3\mu$.[16] This leads to the following expression for the number concentration of the average aggregates $N_{\bar{k}}$

$$\frac{dN_{\bar{k}}}{dt} = -\frac{8k_BT}{3\pi\mu}N_{\bar{k}}^2(t) = -\frac{1}{\tau_A}\frac{N_{\bar{k}}^2(t)}{N_F} \qquad (11)$$

where the subscript $\bar{k}$ indicates the mass of the average aggregate in the system. Conservation of mass requires that

$$N_{\bar{k}}\bar{k} = N_F,\ \frac{dN_{\bar{k}}}{dt} = -\frac{N_F}{\bar{k}^2}\frac{d\bar{k}}{dt}$$

which allows us to recast Eq. 11 in terms of $\bar{k}$ as follows

$$\frac{d\bar{k}}{dt} = \frac{1}{\tau_A} \qquad (12)$$

thus, leading to the following expression of the average aggregate size as a function of time

$$\bar{k}(t) = 1 + t/\tau_A \qquad (13)$$

Once we can predict the time evolution of the average mass, it is necessary to define a proper criterion for gelation, so as to obtain an estimate of τ_G. Among the simplest gelation criteria is the one that identifies the occurrence of colloidal gelation as the time when the fraction of the volume occupied by the aggregates is of the order of 1[17]:

$$\frac{4}{3}\pi R_{\bar{k}}^3 N_{\bar{k}}(t = \tau_G) \approx 1 \qquad (14)$$

where $R_{\bar{k}}$ is the average radius of the aggregates in the system. Accordingly, by means of Eqs. 13 and 5 we can give the following estimation of τ_G

$$\tau_G \approx \tau_A(\phi_F^{-[d_f/(3-d_f)]} - 1) \qquad (15)$$

A typical value for d_f in fully destabilized conditions is about 1.8,[16] and from Eq. 15 we can see that in the range of $\phi_F = 0.1$–0.3 the ratio τ_G/τ_A takes values roughly between 5 and 30. It follows that in conditions where $\tau_M/\tau_A \gg 1$ the characteristic time of gelation can well be of the same order or smaller than τ_M. Thus, we can conclude that in conditions where aggregation is mixing controlled, such as those typical of industrial operations, it is very likely that in a very small latex volume, whose disruption is governed by mixing, the aggregates grow several orders of magnitude in size and eventually gelate, so that the entire volume is occupied by a single aggregate.

Focused Beam Reflectance Method

Focused beam reflectance method (FBRM) allows for convenient online and *in situ* monitoring of particulate systems up to very high solid content, especially if compared with scattering techniques. The measurement device consists of a tubular probe which can be inserted directly into the vessel. A highly focused rotating laser beam illuminates the system through a sapphire window located at the tip of the probe. When the path of the laser beam crosses a particle with sufficient optical contrast with respect to the suspending medium, the backscattered light is collected through the same sapphire window. From this and the knowledge of the laser rotational speed, the

length of the path traveled by the laser across the particle can be calculated. This task is performed by the electronic discrimination circuit of the device, which analyzes the backscattering signal spanning the measurement time and sorts the traced path length into chord bins so as to give as output the so-called chord length distribution (CLD) of the polymer particles.[20,21] To within a proportionality constant (depending only on aggregate shape and structure), moments of the CLD can be transformed into moments of the ASD as follows[22]

$$\mu_{j+1}^{l} = \alpha_j \frac{\mu_j^c}{\mu_{-1}^c} \tag{16}$$

where μ_i^l represents the i-th moment of the ASD, μ_j^c the j-th moment of the CLD and α_j is a proportionality constant depending on j and on the aggregate structure. Eq. 16 was used to extract the following weighted averages of the ASD from the measured CLD

$$d_{4,3} \equiv \frac{\mu_4^l}{\mu_3^l}, \quad d_{1,0} \equiv \frac{\mu_1^l}{\mu_0^l}$$

which for a spherical shape read

$$d_{4,3} = \frac{32}{9\pi}\frac{\mu_3^c}{\mu_2^c} \quad d_{1,0} = \frac{\pi}{2}\frac{\mu_0^c}{\mu_{-1}^c} \tag{17}$$

Experimental

The polymer latex used for the aggregation experiments was a PVDC dispersion type PV-324 provided by Solvay Solvin France S.A. The primary particle diameter was found by dynamic light scattering (Zetasizer 5000, Malvern Instruments) to be 90 nm with a nearly monodisperse particle-size distribution. Solid volume fractions were measured by gravimetry (HG53 Halogen Moisture Analyzer, Mettler Toledo). Throughout all the experiments demineralized water was used for required dilutions or salt solution preparations. Aluminum nitrate nonahydrate (Fluka) was used to induce aggregation. The corresponding CCC was estimated through static aggregation experiments to be $\sim$0.02 g/l.

The first series of aggregation experiments was performed in a jacketed stirred glass vessel (nominal volume 9 l) equipped with two Rushton turbines. Experiments were run as follows. The vessel was filled with two liters of foot solution of salt at concentration C_S' at a temperature of 5°C, which is below PVDC's glass transition temperature. While the stirrer was set to rotate at the desired speed S, stock latex at volume fraction of $\phi_F = 0.111$ and temperature of 5°C, and salt solution at concentration C_S' were fed into the system at flowrates Q_L and Q_S, respectively, until the total volume of 8 l was reached with the final volume fraction. Feeding was implemented by means of peristaltic pumps. The feeding pipe (internal dia. 3 mm) was placed vertically into the vessel. The pipe's outlet was positioned at the upper part of the discharge zone of the lowest impeller and in the middle between the vessel wall and the impeller tip. Weighting of the feed reservoir during the feeding process provided accurate measurements of the feed flow rates. Q_L and Q_S were chosen so as to reach the desired final volume fraction ϕ, whereas the value of C_S' was determined by requiring the coagulant concentration to be above the critical coagulation concentration (CCC) during the whole feeding process as detailed below. In all the experiments the feeding lasted 55 min, and the system temperature was kept between 5°C and 10°C. After the feeding process was finished, the system was left to reach steady state.

Jacket temperature was then set to 90°C, and the vessel temperature reached 75–78°C. This was done to induce polymer crystallinity in order to impart desirable physical properties. The vessel was then cooled down by setting the jacket temperature to 25°C. Eventually, water was filtered out and the resulting wet powder was vacuum dried at 40°C.

Based on the procedure described earlier, once the final volume fraction, ϕ and salt concentration, C_S are chosen, all the remaining operating conditions can be calculated through the following material balances

$$Q_L \Delta t_F \phi_F = V_T \phi$$

$$(Q_L + Q_S)\Delta t_F = V_T - V_F$$

$$C_S'(\Delta t_F Q_S + V_F) = (1 - \phi) V_T C_S$$

that solved for the unknowns Q_L, Q_S and C_S' lead to

$$Q_L = \frac{\phi V_T}{\phi_F \Delta t_F} \tag{18}$$

$$Q_S = \frac{V_T - V_F}{\Delta t_F} - Q_L \tag{19}$$

$$C_S' = \frac{(1 - \phi)\phi_F}{\phi_F - \phi} C_S \tag{20}$$

where V_T and V_F are the final and foot volumes, respectively, Δt_F is the feeding time and for C_S a value of 1 g/l was taken as a conservative choice so as to ensure that the salt concentration is always well above CCC. It can be readily seen that in this setup the latex feeding rate Q_L is proportional to the final volume fraction ϕ. This situation, which is representative of the operating mode of semibatch industrial coagulators, has the disadvantage that both the fluodynamics conditions in the vessel and the aggregate concentration change simultaneously, thus, making it difficult to decouple their effects. For this reason a second experimental setup has been devised where these effects could be studied independently.

The second series of experiments was performed in a jacketed stirred glass vessel (nominal volume 6 l) equipped with one Rushton turbines. The vessel was operated full, so that the liquid level always reached the upper metal flange, so as to avoid the presence of air. This was achieved by pumping only latex at the desired volume fraction ϕ_F, and feed flow rate Q_L into the coagulator already full of salt solution above CCC. Water was allowed to flow out through a filtered outlet so as to keep the particles inside, and the vessel always full. In all the experiments the system volume was 8.88 L. The feeding process lasted until the final solid volume fraction, ϕ was reached.

Table 1. Operating Conditions in the First Experimental Setup

Exp.	Series	$\phi \cdot 10^2$	$Q_L \cdot 10^2$ [l/min]	$Q_S \cdot 10^2$ [l/min]	S [rpm]
1	A	7.72	8.33	0.572	165
2	A, B	7.68	8.20	0.565	410
3	A	7.37	9.53	0.596	645
4	C	0.0910	0.106	9.98	165
5	C, B	0.102	0.135	9.77	410
6	C	0.0912	0.121	9.74	645
7	B	0.945	1.28	9.92	410

In all the experiments the remaining operating parameters were fixed as follows: $\Delta t_F = 55$ min, $\phi_F = 0.111$, $V_T = 8$ l and $V_F = 2$ l.

As soon as the feeding stage was over, the system was left to equilibrate before the heating procedure was performed, as in the previous experimental setup. The initial salt concentration in the vessel was calculated so as to give a salt concentration well above CCC at the end of the feeding process.

In all the experiments the aggregate-size distribution was monitored online by means of the sensor Lasentec FBRM D600L (Lasentec, Redmond, WA), with electronic discrimination circuit set to "C," and the laser focus point left at the factory default, placed inside the vessel just above the discharge zone of the lowest impeller.

Results and Discussion

Experimental results

As a first experimental result, it is convenient to consider the pictures in Figure 2 which show the first instant of time where the latex is entering the salt solution inside the vessel through the vertical tube. Figure 2a and Figure 2b correspond to the experimental runs 17 and 22 of series E in Table 2, respectively, where the operating conditions, which are near to those of industrial interest, probably correspond to the smallest value of the ratio between the characteristic times of aggregation and mixing, τ_A/τ_M. The white plumes indicate that aggregation is so fast that, before the latex volumes can be broken down to the Kolmogorov scale, not only aggregation, but most likely gelation of the entire mass has occurred. This indicates that we are dealing with a process strongly affected by mixing at the small scales of turbulence, where, therefore, the conditions inside the vessel are not uniform. In particular, at least at the high volume fractions considered in Figure 2, aggregation/gelation occurs almost instantaneously as the latex enters the vessel, and the rest of the process is then devoted to breaking down the so formed gel flocks. This has to be accounted for when interpreting the experimental results that we are going to discuss next.

Table 2. Operating Conditions in the Second Experimental Setup

Exp.	Series	$Q_L \cdot 10^2$ [l/min]	$\phi \cdot 10^2$	$\phi_F \cdot 10^2$	τ_A/τ_M	τ_G/τ_M
8	D	5.51	1.23	1.10	17.4	0.0201
9	D	6.12	1.23	1.10	17.4	0.0201
10	D	7.94	1.23	2.44	38.6	0.148
11	D	7.95	1.23	4.39	69.4	0.645
12	D, E	6.63	1.23	11.0	174	6.59
13	D	7.18	1.25	20.0	316	31.1
14	D	7.04	1.25	28.0	443	77
15	D	5.82	1.25	28.6	452	81.7
16	D	6.08	1.25	28.6	452	81.7
17	E	3.30	1.23	11.0	174	6.59
18	E	3.03	1.35	12.0	190	8.23
19	E	3.12	1.35	12.0	190	8.23
20	E	2.95	1.35	12.0	190	8.23
21	E	11.0	1.23	11.0	174	6.59
22	E	14.2	1.23	11.0	174	6.59
23	F	14.3	1.82	28.6	452	81.7
24	F	15.2	4.91	28.0	443	77
25	F	12.8	9.22	28.6	452	81.7

In all the experiments the remaining operating parameters were fixed as follows: $V_T = 8.88$ l and $S = 165$ rpm.

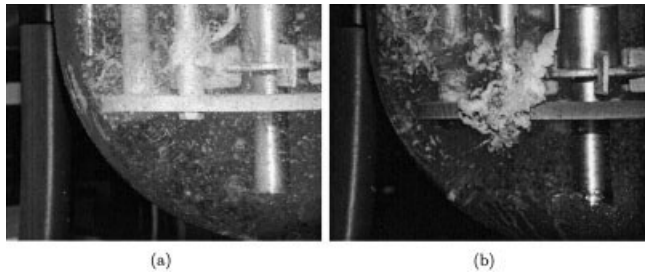

Figure 2. Snapshot of the latex feed entering the vessel at the very early stage of feeding.

(a) Experimental run 17 of series E in Table 2. (b) Experimental run 22 of series E in Table 2.

First experimental setup

For what concerns the behavior of the system in the first setup at steady state before the heating phase, as seen in Table 1, all the experiments were run at the same feeding volume fraction, $\phi_F = 11.1\%$ and feeding time, $\Delta t_F = 55$ min. On the other hand, various values of the final volume fraction ϕ, and the stirring speed S have been investigated, while the flow rates, Q_L and Q_S have been changed according to Eqs. 18 and 19. Figure 3 shows each experiment as a point in the $\phi - S$ plane, where dashed circles indicate the series to which each experiment belongs. In series A the experiments were run at a

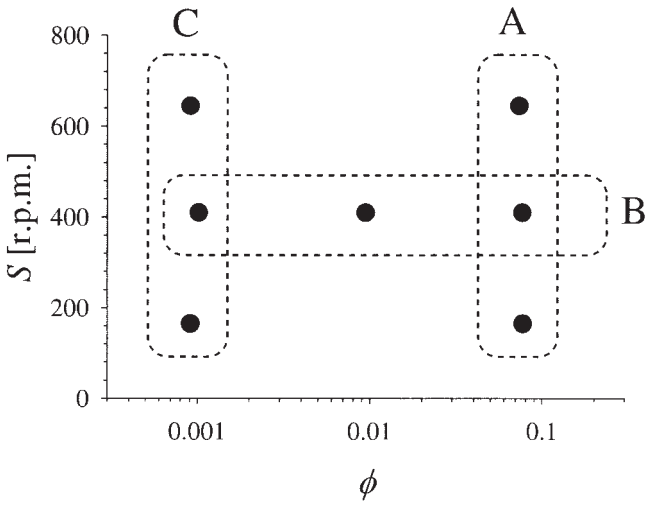

Figure 3. Experimental conditions of the experiments carried out in the first experimental setup.

Dashed circles indicate the series to which each experiment belongs.

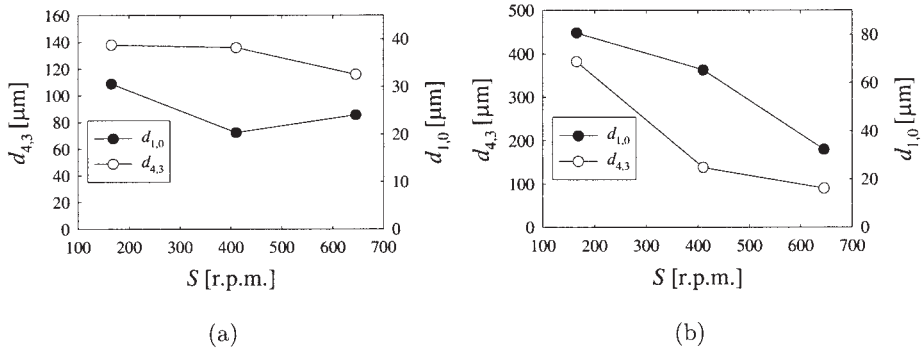

Figure 4. Volume and number weighted average size as a function of stirring speed for the aggregation experiments run in the first experimental setup.

(a) Series A: $\phi \simeq 7.5 \cdot 10^{-2}$. (b) Series C: $\phi \simeq 9.5 \cdot 10^{-4}$. Lines are drawn to guide the eye.

moderately high final volume fraction of about 7.5%, while three values of the stirring speed were investigated. Figure 4a shows the measured volume weighted average dia. $d_{4,3}$ (circles, left-axis scale) and number weighted size (filled circles, right-axis scale) as a function of the stirring speed S. It is seen that both average sizes are relatively insensitive to the variations of the agitation in the system. The situation radically changes for the experiments performed at a low final solid volume fraction of $\phi \simeq 9.5 \cdot 10^{-4}$, that is series C in Figure 3. As shown in Figure 4b, in these conditions the increase of the stirring speed results in a marked decrease of both the volume, and the number weighted sizes. This is consistent with results reported in the literature for dilute systems, where $d_{4,3} \sim \varepsilon^{-0.5}$ is often observed in turbulent conditions.[23] The ratio of $d_{4,3}$ to $d_{1,0}$, which is a measure of the polydispersity of the size distribution, decreases from a value of 4.7 to 2.8, when S changes from 165 to 645 rpm. This means that the decrease in size is accompanied by narrowing of the ASD. These observations indicate that, as the volume fraction in the system is increased from very diluted to concentrated conditions, a fundamental change in the aggregation/breakage mechanism occurs. While at high volume fractions the change in the aggregation rate due to the increase in the stirring speed seems to be balanced by a similar change in the breakage rate, this balance seems to no longer hold at low volume fractions.

In the series B of experiments we fixed the stirring speed at the intermediate value of 410 rpm and let the final volume fraction change between the two values used in the previous two series. The results are shown in Figure 5a, where volume and number weighted sizes, $d_{4,3}$ are plotted against the solid volume fraction ϕ. It is seen that $d_{4,3}$ does not change significantly as the volume fraction increases and retains a value close to the smallest one measured in the previous series of experiments. On the other hand, the number weighted average size $d_{1,0}$ decreases significantly as ϕ increases. This different behavior of $d_{4,3}$ and $d_{1,0}$ is consistent with an increase of the fraction of fines at higher solid volume fractions. However, we should observe that, due to the specific characteristic of the adopted setup described earlier, the final volume fraction in the system is proportional to the latex feed flow rate. This means that, in the experiments at higher final solid volume fractions, a larger feed flow rate has been used. Therefore, in these experiments we cannot decouple the effects of mixing and aggregate concentration. This issue is addressed in the second series of experiments where operating the vessel full and using a filter at the outlet allows us to decouple the feed rates from the final solid volume fraction in the system.

As far as the transient behavior of the system is concerned, it is interesting to compare the evolution of the cumulative chord-length distribution (CCLD) measured in the experimental runs with low and high-final solid volume fraction (that is, low-latex feed rate). In Figure 6 the CCLDs measured at

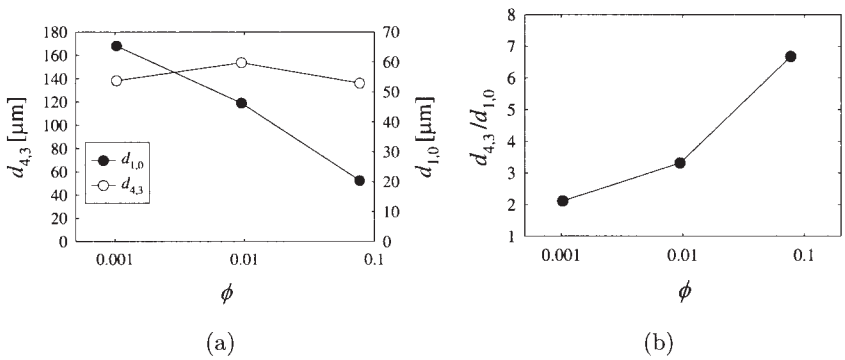

Figure 5. Series B of aggregation experiments: (a) Volume and number weighted average size as a function of the final volume fraction ϕ, (b) Ratio of the volume weighted average size to the number weighted average size $d_{4,3}/d_{1,0}$ as a function of the final volume fraction ϕ.

Lines are drawn to guide the eye.

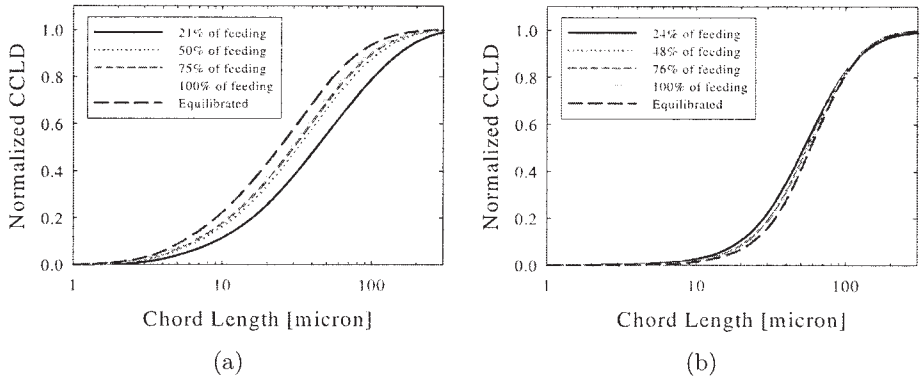

Figure 6. Cumulative chord length distribution (CCLD) normalized to one at various percentages of the feeding time, Δt_F: (a) Experiment 2, $\phi = 7.68 \cdot 10^{-2}$ and $Q_L = 8.20 \cdot 10^{-2}$ l/min; (b) Experiment 5, $\phi = 1.02 \cdot 10^{-3}$ and $Q_L = 1.35 \cdot 10^{-3}$ l/min.

various times are reported for the experiments at $\phi = 7.68 \cdot 10^{-2}$, and $Q_L = 8.20 \cdot 10^{-2}$ l/min (Figure 6a), and at $\phi = 1.02 \cdot 10^{-3}$ and $Q_L = 1.35 \cdot 10^{-3}$ l/min (Figure 6b), that is, experiments 2 and 5 in Table 1, respectively. It is seen that at the higher feed rate the aggregate population moves toward smaller chords as time passes by. Even after feeding is over, this trend continues until the equilibrium distribution is reached. In contrast, at the lower feed rate (Figure 6b) the CCLD remains practically unchanged during feeding and equilibration. In this case the feeding process is so slow that at each instant in time an equilibrium between aggregation and breakage is reached, as it is also demonstrated by the fact that the distribution at the end of the equilibration stage perfectly falls atop of the earlier ones. We should also consider that in this experiment the final solid volume fraction, ϕ is so low that the volume fraction in the system changes very little, which explains why the CCLD remains constant also during the feeding stage. On the other hand, in experiment 2 the volume fraction in the system changes substantially in time, thus, the fact that the CCLD continues to move to the left even after the feeding is over until equilibrium is reached indicates that the system is not at steady state, and the equilibration stage is further shifted to the left.

Second experimental setup

In Table 2 the operating conditions used for the second experimental setup are reported. In all the experiments the stirring speed was fixed at 165 rpm. Figure 7 shows each experiment, as a point in the $\phi_F - Q_L$ plane, and all the experiments may be classified into two series D and E, as indicated by the dashed circles. In series E, while keeping the feeding solid volume fraction, ϕ_F close to 11%, the latex feed rate Q_L has been varied between 0.03 and 0.14 l/min, with a constant final solid volume fraction $\phi \simeq 1.3\%$. The corresponding measured volume weighted size $d_{4,3}$ (open circles, left-axis scale) and number weighted size $d_{1,0}$ (filled circles, right-axis scale) are plotted vs. Q_L in Figure 8a. We can readily observe a significant decrease of the volume weighted size as Q_L increases, but the effect of Q_L on the number weighted size is insignificant. It follows that the ASD narrows down as Q_L increases. It should be noticed that the experimental runs at the smallest flowrate are basically repetitions of the same experiment. It is seen that the reproducibility of the experiments is good, though the measured $d_{1,0}$ are somewhat more scattered.

Figure 8b shows the results of the experiment series F in Table 2, where at fixed Q_L and ϕ_F around 0.13 l/min and 28%, respectively, the effect of changes in the final solid volume fraction, ϕ on the measured average aggregate sizes has been studied. Note that larger values of the solid volume fractions, ϕ are reached in this case by operating the unit for longer times. Here, we can observe that both average sizes decrease as the final volume fraction in the vessel increases, although the decrease in $d_{1,0}$ is less marked, thus, leading to narrower ASD.

In the last two series of experiments, that is, E and F, the effects of the flowrate, Q_L and the final solid volume fraction have been investigated independently. This can now help to explain the results of the series B of experiments in the first experimental setup, where these two parameters were coupled. In particular, we see that both of them independently produce the same qualitative effect on $d_{1,0}$ and $d_{4,3}$ as they did coupled

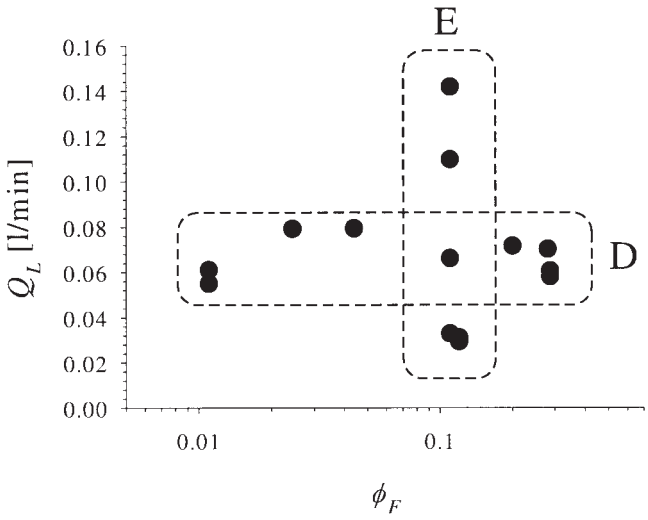

Figure 7. Experimental conditions for the experimental series D and E carried out in the second experimental setup.

Dashed circles indicate the series to which each experiment belongs.

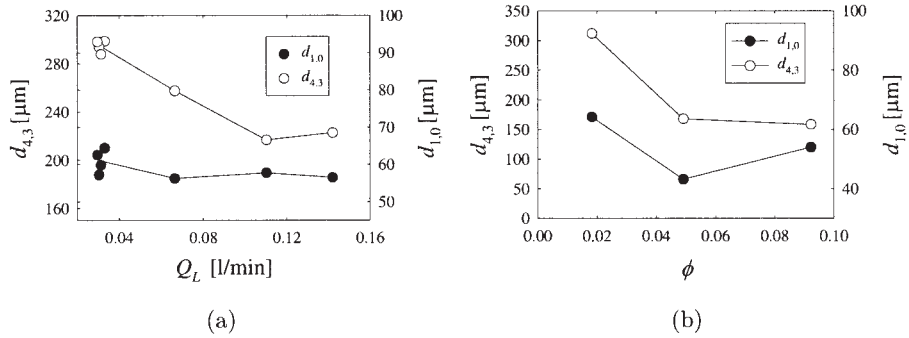

Figure 8. Volume and number weighted average size in the second aggregation setup as a function feed flow rate (a) and final solid volume fraction (b). (a) Series E: $\phi \simeq 1.3 \cdot 10^{-2}$, $\phi_F \simeq 0.11$, and (b) Series F: $Q_L \simeq 0.14$ l/min, $\phi_F \simeq 0.28$.

Lines are drawn to guide the eye.

together in the first setup. However, it should be stressed that, as opposed to series B, where the ratio $d_{4,3}/d_{1,0}$ markedly increased, in series E and F this ratio either remains constant or slightly decreases, respectively. This discrepancy can be explained if we take in consideration that series B was run at higher stirring speed, that is, 410 rpm instead of 165 rpm. It is, in fact, most likely that in this series many big aggregates are broken by the agitation, and, therefore, an increase in ϕ and/or Q_L yields no decrease in the volume weighted average size. This explanation is also supported by the observation that in series B $d_{4,3}$ is never larger than about 140 microns, while in series E and F the same quantity can be as large as 300 microns.

In Figure 9 the measured volume and number weighted average sizes are plotted against feeding volume fraction ϕ_F for the data in series D. Here the final solid volume fraction was fixed at the smallest explored value, that is $\phi \simeq 1.23\%$, while for the feed flow rate an intermediate value was chosen, that is $Q_L \simeq 0.06$ l/min. We see that both sizes significantly grow as the feeding volume fraction increases over one order of magnitude until values typical of industrial operation are reached. Runs at the highest feeding volume fractions were essentially repetitions of the same experiment. As for series E we observe that reproducibility of $d_{4,3}$ is good, while $d_{1,0}$ data are somehow scattered.

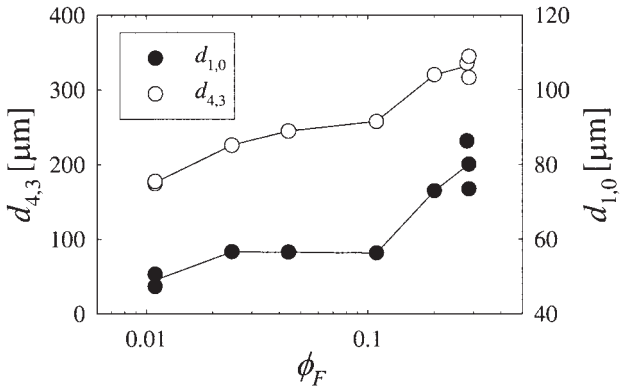

Figure 9. Volume and number weighted average size as a function of feed solid volume fraction for the aggregation experiments run in series D: $\phi \simeq 1.23 \cdot 10^{-2}$, $Q_L \simeq 6 \cdot 10^{-2}$ l/min.

Lines are drawn to guide the eye.

Interpretation of the Experimental Results

As discussed in the modeling section in the context of Figure 1, for the operating conditions considered in this work we expect a substantial effect of the fluodynamic conditions on the aggregation process. It is actually rather obvious that, if the process were not mixing controlled, no dependency other than that on the final solid volume fraction should be expected, while the data above show a significant dependence on the feed solid volume fraction and flow rate. In particular, the results reported for series D and E clearly demonstrate the interplay between mixing and aggregation. Another element supporting this statement is brought by the visual observation of the latex streams entering the vessel during an aggregation experimental run. In Figure 2 two snapshots taken at the very beginning of the latex feeding process for the experimental runs 17 (Figure 2a) and 22 (Figure 2b) of series E in Table 2 are shown. We notice a white plume coming out of the feed pipe whose boundaries are frozen in by the gelation process, and become millimeter sized aggregates. This indicates not only that aggregation is faster than mixing, but that even gelation occurs on time scales smaller than those of mixing at the local scales. A similar behavior was observed in all the experimental runs, where the feed concentration was sufficiently high and/or the feed flow rate sufficiently low. In the opposite situation the plume boundaries are not frozen in by gelation and gradually fade as their lengthscale is further broken down by the mixing process. This behavior is illustrated in Figure 10, where a snapshot taken at an early instant of time in the feeding process of a very diluted latex (experimental run 8 of series D in Table 2) is shown.

In order to quantitatively support these observations let us analyze the relevant timescales for our experimental conditions. Computational fluid dynamics (CFD) simulations enabled us to estimate the rate of energy dissipation in the vicinity of the feed point (see Appendix for details), and from this the corresponding value of the Kolmogorov microscale η at a stirring speed $S = 165$ rpm

$$\eta \equiv \left(\frac{\nu^3}{\varepsilon}\right)^{1/4} \simeq 50\ \mu\text{m}$$

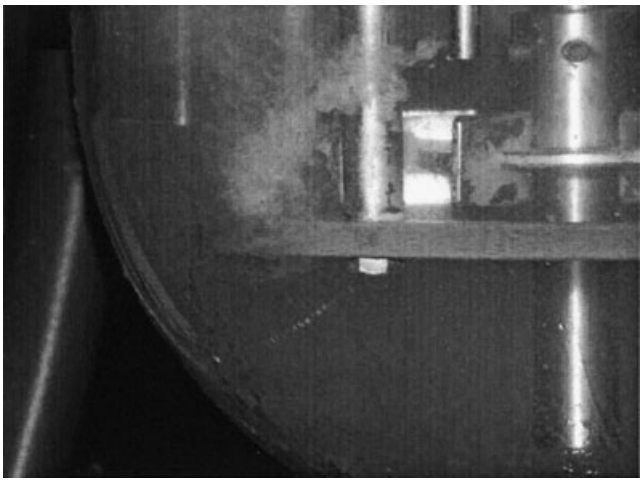

Figure 10. Latex feed at very low-solid volume fraction entering the vessel at the very early stage of feeding for the experimental run 8 of series D in Table 2.

This value is below the average aggregate sizes observed in the experiments reported earlier, which suggests that mixing at scales larger than the Kolmogorov microscale (the so-called mesoscale) could play a role. On the other hand, it has been shown that the most active transient vortices involved in the process of micromixing have a typical size around 12η,[24,25] which in our case falls around 600 μm, and is above the average sizes observed. This seems to indicate that both mixing mechanisms could affect the experimental observations. Consequently, we will consider both mechanisms in the interpretation proposed in the following.

If we assume inertial convective disintegration of large eddies as the main mechanism acting in reducing the lengthscale of particle concentration fluctuation to the Kolmogorov scale, then the corresponding mesomixing timescale is given by[24,26]

$$\tau_{\text{meso}} = 2\Lambda_c^{2/3}\varepsilon^{-1/3} \tag{21}$$

where, Λ_c is the characteristic lengthscale of the feed stream. If the linear velocity in the feeding pipe, u_p is much larger than the average velocity near the feed point, $\bar{u}$ (jet conditions) Λ_c is equal to half of the diameter of the pipe d_p, and the rate of energy dissipation ε can be estimated as follows[27]

$$\varepsilon = \frac{u_p^3}{d_p} \tag{22}$$

In the opposite case (nonjet conditions) the momentum of the entering stream is very low, and it instantaneously adjusts to the average velocity in the vicinity of the feed point $\bar{u}$. An upper-bound approximation of $\bar{u}$ is given by the impeller tip velocity. In this case the characteristic length Λ_c can be computed as the size of the stream that, at linear velocity $\bar{u}$, gives the feed flow rate Q_L, that is

$$\Lambda_c = \sqrt{\frac{Q_L}{\pi\bar{u}}} \tag{23}$$

In the conditions adopted in the series of experiments D and E the ratio $u_p/\bar{u}$ ranged from 0.1 to 0.43, and, therefore, we do not always have clear jet or nonjet conditions, particularly considering that estimating $\bar{u}$ by the impeller tip velocity can yield a value substantially larger than the real one. For this reason in the following we consider two values of characteristic mesomixing times: τ^j_{meso} and τ^{nj}_{meso} corresponding to jet and nonjet conditions as given by the following expressions

$$\tau^j_{\text{meso}} = 2^{1/3}\frac{d_p}{u_p} \tag{24}$$

$$\tau^{nj}_{\text{meso}} = 2\left(\frac{Q_L}{\pi\bar{u}}\right)^{1/3}\varepsilon^{-1/3} \tag{25}$$

respectively. In Figure 11a the two mesomixing characteristic times are shown, together with the gel timescale τ_G given by

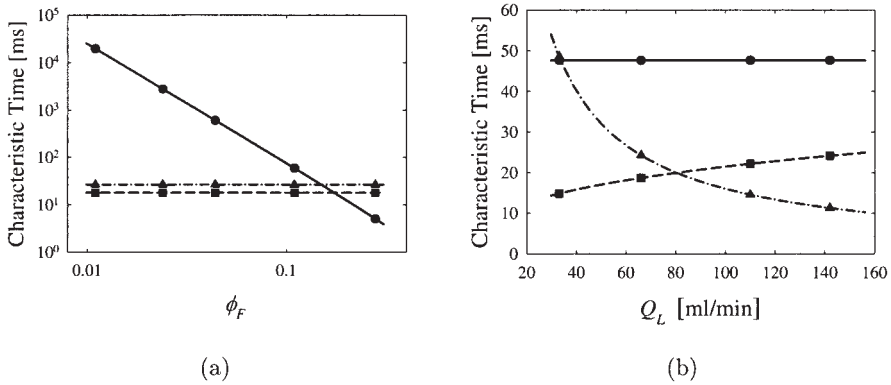

Figure 11. (a) Timescale of gelation τ_G (solid line), mesomixing in jet (dash-dotted line) and nonjet (dashed line) conditions as a function of the feed volume fraction, ϕ_F for the series of experiments D, and (b) Timescale of gelation τ_G (solid line), mesomixing in jet (dash-dotted line) and nonjet (dashed line) conditions as a function of the feed flow rate, Q_L in conditions corresponding to the series of experiments E.

Symbols are used to indicate points where experiments were run.

Eq. 15, as a function of the feed solid volume fraction, ϕ_F for the experimental conditions corresponding to the series of experiments D in Table 2. It is seen that the two mesomixing times are quite similar and that for small feed volume fractions, ϕ_F the characteristic time of gelation, τ_G is orders of magnitude larger than the mesomixing time. However, as the feed solid volume fraction increases the gelation timescale decreases while the mesomixing ones remain constant, so that a crossover occurs at $\phi_F \simeq 10\%$. This implies that at very small ϕ_F values, the latex stream entering the vessel has time to spread over the entire system volume before Brownian aggregation, and, subsequently, shear aggregation start to be significant. In this case, the system tends to be uniform and a dynamic equilibrium is then reached when the average aggregate size is large enough to bring about aggregate breakage. As the feed volume fraction is increased, Brownian aggregation gradually becomes faster than mixing, thus taking place at volume fractions larger than those that would be obtained if the latex would have been uniformly spread on the entire vessel through mixing. Hence, gelation freezes in aggregates in a denser structure that enables them to better withstand shear stresses, leading to aggregate sizes larger than those obtained at the same final solid volume fraction, ϕ and smaller feeding volume fractions ϕ_F. This agrees with the measured aggregate sizes increasing with ϕ_F shown in Figure 9. It should be noted that another physical phenomenon could play a role in the observed increase of the average size with the feed volume fraction. The fact that the mesomixing characteristic time is larger than the gelation characteristic time means that the turbulent flow has not enough time to bring the feed stream lengthscale, Λ_c down to the Kolmogorov microscale by means of the stretching and folding mechanism. This implies that the final average aggregate size corresponds to the size reached by the feed stream length scale during the stretching and folding at the moment where gelation occurs and freezes in the aggregate structure. Obviously, earlier gelation (which means higher ϕ_F) will freeze in larger structures.

This last argument can be used also to explain the results observed in the experimental series E. Figure 11b, shows the corresponding gel timescale τ_G and the mesomixing timescale in jet, τ^j_{meso} and nonjet, τ^{nj}_{meso} conditions as a function of the feed flow rate Q_L. Here we should stress that the estimate for the gelation characteristic time, τ_G given in Eq. 15 neglects the contribution of shear to aggregation. Since the shear aggregation rate scales with the volume of the aggregates (cf. Eq. 3) this could lead to a substantially shorter gelation time scale. We see that while the mesomixing time in jet conditions decreases as the feed rate increases, the mesomixing time in nonjet conditions, instead, increases. In the former case larger Q_L values imply larger momentum values which lead to larger local energy dissipation rates (Eq. 22) and, consequently, shorter mixing times (Eq. 24). In the latter case larger feed flow rates produce larger characteristic lengths, Λ_c (Eq. 23) of the stream entering the vessel, which then takes more time to be reduced to the Kolmogorov microscale by the turbulent flow (Eq. 21). On the other hand, the aggregation/gelation characteristic time is not affected by the feed flow rate.

In this case it is obviously difficult to draw conclusions since, with the simple expressions used in this article to describe mesomixing, we cannot sufficiently characterize the local fluodynamics around the inlet of the feed stream. We can say *a posteriori* that, based on the arguments developed in the context of Figure 11b, the system should be better described by a jet model, since in this case as Q_L increases τ^j_{meso} decreases, which means that the process of jet disrupture is faster, and, since the gelation process takes always the same time, it follows that the aggregate size decreases as shown in Figure 8a. To further support this instance, it is useful to analyze the jets portrayed in Figure 2. Figure 2b shows the latex feed stream entering the vessel in one of the experimental runs at the highest feed flow rate explored in the second experimental setup, that is, $u_p/\bar{u} \simeq 0.43$. We notice that the latex flow is hardly affected by the flow field found in the vessel. Indeed, since the feed point is placed slightly above the discharge zone of the impeller, if the latex stream would adjust to the flow filed in the vessel it should move horizontally slightly upwards. This corroborates our hypothesis that, at least at the highest feed flow rates, the feed is in jet conditions. At the smallest feed flow rate explored, that is, $u_p/\bar{u} \simeq 0.1$, the situation is less clear as shown by the snapshot in Figure 2a. Here, we notice that the length traveled by the latex stream following the direction of the feed pipe is substantially shorter than that in the previous case, even though it is not negligible as nonjet conditions would require.

In the discussion earlier, we considered only the mixing process occurring on the mesoscale, based on the observation that the average aggregate sizes measured experimentally fall above the Kolmogorov scale calculated through CFD simulations. However, owing to the increase of viscosity caused by the suspended phase, the Kolmogorov scale could be actually larger than the given estimate. In this situation the mechanism of mixing due to energetically active small scale motions (that is, micromixing) is radically different from that acting on the mesoscale and discussed earlier. It is worth then to discuss the experimental observations in the frame of micromixing. A widely adopted model for micromixing is the so-called engulfment, deformation, diffusion (EDD) model.[24,25,28,29] According to this model the main mechanism of micromixing is due fluctuating vorticity. Vortices engulf ambient fluid, thus, forming partially segregated laminae of initial size η which are stretched while diffusion transports chemical species across the laminae, thus, allowing for chemical reaction. When a time τ_ω is reached the vortices return to isotropy and new laminae are formed. This process repeats itself at a frequency τ_ω^{-1}, while the number of laminae follows a geometric progression of ratio 2. The process lasts until reaction is complete. The size of the vortices is assumed to be $\sim 12\eta$ which corresponds to the shortest time to regain isotropy $\tau_\omega \simeq 12.7(\nu/\varepsilon)^{1/2}$. Within this description of mixing at the small scales an important characteristic time is that of diffusion into a shrinking slab τ_{DS} which is given by

$$\tau_{DS} = 2\left(\frac{\nu}{\varepsilon}\right)^{1/2} \operatorname{arcsinh}(0.05\ \text{Sc}), \tag{26}$$

where $\text{Sc} \equiv \mu_t/\rho D$ is the Schmidt number with D representing the diffusion coefficient, and ρ and μ_t, the density and viscosity of the suspension, respectively. When Sc is much smaller than 4,000, and the diffusion coefficients of the chemical species are not substantially different, engulfment becomes limiting, and the EDD model can be further simplified into what is known as

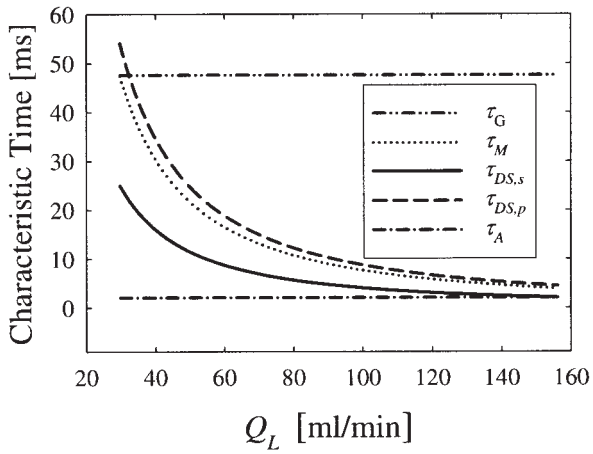

Figure 12. Characteristic times relevant to the interplay between micromixing and aggregation/gelation plotted vs. the latex feed flow rate, Q_L in conditions corresponding to the series of experiments E: Characteristic time of aggregation, τ_A (dash-dotted line), characteristic time of gelation, τ_G (dash-doubledotted line), micromixing time, τ_M (dotted line), characteristic time of salt diffusion across a shrinking slab, $\tau_{DS,s}$ (solid line), characteristic time of primary particle diffusion across a shrinking slab, $\tau_{DS,p}$ (dashed line).

the E-model.[30] The resulting characteristic micromixing time scale is then given by Eq. 9 and corresponds to the time scale of fluid engulfment. Within this description of micromixing, we will have to accommodate salt diffusion from the engulfed lamellae into latex lamellae, aggregation/gelation and aggregate diffusion out of latex lamellae. It is important to stress that, as opposed to the case of standard chemical reactions, in our case the fluodynamic is affecting not only the mechanism of micromixing but also the aggregation rate equations. As a consequence interpretation of experimental results is less straightforward than in the case of chemical reactions.

In our situation, the Schmidt number for the salt falls well below 4,000, therefore, salt transport into the latex is limited by engulfment. This, however, doesn't ensure that aggregation will occur in homogeneous conditions within the latex lamellae, indeed the salt concentration in the median plane of the lamella will reach the CCC after a time $\tau_{DS,s}$ (given by Eq. 26 substituting the diffusivity of the salt) has elapsed since the lamella has been formed. In concentrated conditions this time might result longer than the characteristic time of aggregation τ_A. This is illustrated in Figure 12 where several characteristic times related to micromixing and aggregation/gelation are plotted against the latex feed flow rate, Q_L for conditions corresponding to those of the series of experiments E. Here we notice that $\tau_{DS,s}$ (solid line) is always larger than τ_A (dash-dotted line) as foreseen. This wouldn't affect the final result if particle would diffuse out at the same rate as the salt diffuses in. However, the dashed line in Figure 12 shows that this is not the case since the characteristic time of primary particle diffusion across the lamella, $\tau_{DS,p} \equiv 2(\nu/\varepsilon)^{1/2}\text{arcsinh}(0.05D_1/\rho\mu_t)$ is relatively larger than $\tau_{DS,s}$. We should also note that, as particles aggregate and grow, their diffusion coefficient decreases, thereby, further substantiating the previous statement. The net result is that in our case the EDD model cannot be simplified to the E-model and, consequently, both the time of engulfment (or micromixing time) τ_M and $\tau_{DS,p}$ have to be considered in the interpretation of our experimental results.

As indicated earlier, it is reasonable to assume that in the series of experiments E the latex feed stream is in jet conditions at least for high latex feed flow rates. Accordingly, we plotted in Figure 12 the characteristic times related to micromixing assuming jet conditions in the latex feeding stream. Always bearing in mind that the right value for the characteristic time of gelation, τ_G (dash-doubledotted line) might be smaller, we see that at low Q_L gelation is faster than aggregate diffusion across the slab. Hence, the lamellae formed during salt engulfment and gelation are frozen to the size reached by stretching during this time span. As Q_L increases the rate of stretching of the laminae increases causing the gelation to freeze in smaller structures. Further increases of the latex feed flow rate result in shorter aggregate diffusion times over the lamellae. Therefore, at some point the aggregates are able to diffuse over the engulfment volume before gelation occurs. In this case aggregates are formed in more dilute conditions most likely result in less denser structures. This interpretation is in agreement with the initial decrease of the volume weighted average size observed in series of experiments E and reported in Figure 8a.

We should stress that the arguments given above are intrinsically of qualitative nature and, therefore, have to be used only as a guide for our understanding. For a quantitative interpretation of these results CFD tools coupled with suitable models of mixing at all scales, and a rigorous model for the aggregation/gelation process should be used. This is, however, beyond the scope of this experimental investigation.

For what concerns the effect of the final solid volume fraction, ϕ illustrated in Figure 8b the observed decrease of the average sizes is in contrast with what reported in Ref. [31] where the aggregation and breakage of polystyrene aggregates of 1 μm dia. in agitated vessels was studied and an increase in the

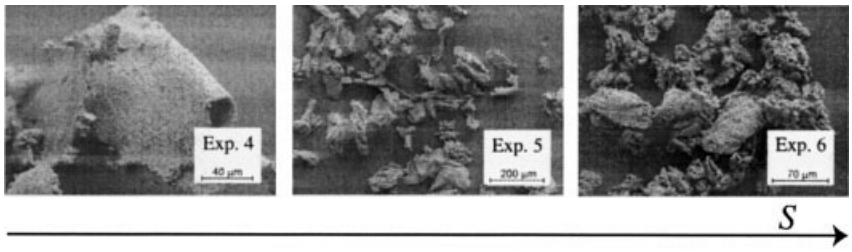

Figure 13. SEM pictures: experiment number as in Table 1.

average size was observed. However, it should be pointed out that, owing to the adopted light scattering sizing technique, the maximum explored solid volume fraction was about $2 \cdot 10^{-3}$ which is one order of magnitude smaller than the minimum value investigated in this work. In these conditions mixing is presumably faster than aggregation and the system is then uniform. Accordingly, an increase of aggregate size with solid content would be justified owing to the fact that aggregation and breakage follow second and first-order kinetics, respectively. Even if one would speculate that there exists a critical size above which the aggregation rate drops to zero due to inertial effects or to the fact that breakage events are correlated to aggregate encounters, still only a plateau would be justified, but not a decrease of the aggregate size as the one observed in Figure 8b. We must consider, though, that at high solid volume fractions, such as those investigated in this work, the flow alteration of the continuous phase produced by one aggregate is felt by the others. The net result is that the viscosity of the suspension increases with volume fraction, so that for a given shear rate (or equivalently a stirring speed) the shear stresses acting on each aggregate increase with solid volume fraction.[32] This leads to an apparent order of the breakage kinetics which is larger than two and could justify the decrease of the aggregate size shown in Figure 8b.

In light of the discussion above, we can further analyze the transient behavior observed in the first experimental setup and illustrated in Figure 6. Due to the high feed volume fraction, latex volumes entering the vessel are immediately aggregated and gelled into millimeter sized aggregates, which are, subsequently, broken to the equilibrium size. Since simple breakage is a first-order process, its characteristic time is independent of volume fraction, and remains constant as long as the stirring speed is kept fixed. As a consequence, the dynamics of the aggregate size distribution is controlled by the relative magnitude of the breakage characteristic time, and the rate at which gel aggregates appear in the vessel, which is clearly proportional to the rate at which latex is fed into the vessel. In particular, for the large feed flow rate adopted in experiment 2 in Table 1, breakage is too slow compared to the rate at which gel aggregates are entering the vessel. Therefore, after stopping the feed, breakage is able to shift the aggregate-size distribution towards smaller sizes, thus, achieving the steady state corresponding to the current conditions in the system as shown by the experimental data in Figure 6a. On the other hand, for the low-feed flow rate used in experiment 5 in Table 1, breakage is sufficiently fast to achieve, at every instant, the same pseudosteady-state conditions, which lead to the constant aggregate-size distribution shown in Figure 6b. In this case of course no change occurs in the CCLD after stopping the feed.

A final confirmation of the analysis reported above comes from the scanning electron microscopy (SEM) pictures of the final aggregates collected for the experimental runs 4, 5 and 6 in Table 1, that is, series C in Figure 3, where at $\phi_F = 0.111$ the stirring speed increases from 165 rpm to 645 rpm. We can observe very clearly the lamellar structure of the sample at the smallest stirring speed, which supports our understanding that the latex volume, after being stretched and folded, was frozen in the resulting lamellar shape by gelation. Subsequent moderate agitation in the vessel was not able to destroy the resulting structure. Upon increase of agitation it is evident that the same lamellar structure is gradually destroyed. It should be noted that these results indicate that the morphology of the aggregates is not affected by the softening of the polymer induced by the heating stage above the glass transition temperature. Most probably at the particular heat rate we imposed to the system, the softening could only act on length-scales smaller than those of the mixing layers before hardening due to crystallization became significant.

Conclusions

By means of very simple relations based on the relevant characteristic times the kinetics of micromixing and of aggregation and gelation for fully destabilized polymer latex in stirred vessels have been investigated. It is shown that, in industrially relevant conditions (that is, volume fractions above 10% and primary aggregate sizes below 200 nm), latex aggregation, and even gelation are complete before mixing at small scales is achieved. These conditions have been investigated experimentally by feeding an electrostatically stabilized PVDC latex in a stirred vessel operated in a semibatch mode together with a salt solution with concentration above the critical coagulation concentration (CCC). During aggregation the temperature was always kept below PVDC glass transition temperature. The aggregate-size distribution was monitored *in situ* and online by means of the focused beam reflectance method.

In a first experimental setup the salt solution and the latex at 11.1% volume fraction were fed into the system over a fixed time interval. At high volume fractions the steady-state aggregate size was shown to be quite insensitive to the stirring speed. The opposite behavior was observed when the experiments were run at lower solid volume fractions. This observation suggests that a profound change in the aggregation/breakage mechanism occurs as the volume fraction in the system increases. Although this setup reproduces the conditions of the typical industrial coagulation unit, it has the disadvantage that both the fluodynamics (due to the filling in time of the vessel), and the solid volume fraction change continuously during the process.

To avoid this, a second experimental setup has been designed where the three main operating variables: feed flow rate, feed solid volume fraction and final solid volume fraction in the vessel, can be investigated independently. The interpretation of the obtained results is based on the interaction between aggregation/gelation and mixing at small scales. Both mesomixing and micromixing were considered. Care was taken to properly account for the peculiarities of aggregation as opposed to standard fast chemical reaction. A simple estimation of the relevant characteristic times shows that aggregation/gelation and mixing at the small scales are the two competing processes, as it is also confirmed by the plume of gelled latex formed immediately after the entrance of the feed stream in the vessel. The general trend is that when gelation is faster than mixing at intermediate and small scales, the latex volumes gel before the surrounding turbulent flow can break them down to either the Kolmogorov scale in the case of mesomixing, or to scales small enough to allow for diffusion in the case of micromixing. The final size of the aggregates is then determined by the competition between the two processes. They tend to be larger the faster gelation can freeze in the latex volume, and the slower mixing breaks them through the turbulent stretching and folding mechanism. This conclusion is supported by the scanning

electron microscope images of the final aggregates. In the case of the fastest gelation times, that is, at large feed solid volume fractions, they still exhibit a lamellar structure resembling the shape of the fluid folding during mixing at the outlet of the feed pipe. Due to the relative similarity between the micro- and meso-mixing time most probably both mechanisms play a role on the experimental observations. However, considering the approximations involved in the estimation of the relevant characteristic times, these conclusions have to be regarded as qualitative.

Acknowledgments

This work was performed with financial support by the Swiss National Science Foundation (NSF), under Grant No. 200020-101724 and by Solvay. The authors are grateful to Miroslav Šoóš for performing the CFD simulations.

Notation

a = primary particle diam.
$d_{4,3}$ = volume weighted average aggregate size
$d_{1,0}$ = number weighted average aggregate size
d_p = feeding pipe diam.
D = diffusion coefficient
D_i = diffusion coefficient an aggregate of nondimensional mass i
C_S = salt solution concentration in the system
C_S' = salt solution feed concentration
i = nondimensional mass of an aggregate
j = nondimensional mass of an aggregate
k = nondimensional mass of an aggregate
k_0 = prefactor in fractal scaling (Eq. 5)
k_B = Boltzmann constant
K_{ij} = aggregation kernel matrix
K_{ij}^{Brown} = Brownian aggregation kernel matrix
K_{ij}^{Turb} = turbulent aggregation kernel matrix
N_i = number concentration of an aggregate of nondimensional mass i
N_i^F = number concentration of an aggregate of nondimensional mass i in the feed stream
Q_L = latex volumetric feed rate
Q_S = salt solution volumetric feed rate
R_i = size of an aggregate of nondimensional mass i
S = impeller rotational speed
Sc = Schmidt number
t = time
T = temperature
$\bar{u}$ = average velocity near the feed point
u_p = linear velocity in the feeding pipe
V, $V(t)$ = volume of the system
V_F = foot salt solution volume
V_T = final total volume in the vessel

Greek letters

α_j = proportionality constant between CLD and ASD moments (Eq. 16)
β = hydrodynamic parameter appearing in the Stokes-Einstein relationship (Eq. 4)
Γ_k = first-order breakage rate constant
Δ_{ik} = daughter aggregate mass distribution
Δt_F = feeding duration
ε = rate of turbulent energy dissipation
η = Kolmogorov microscale
Λ_c = characteristic lengthscale of the feeding stream
μ = suspending medium viscosity
μ_j^c = j-th order moment of the CLD
μ_j^l = j-th order moment of the ASD
μ_t = suspension viscosity
ν = suspending medium kinematic viscosity
ρ = suspension density
τ_{meso}^j = characteristic time of mesomixing in jet conditions
τ_{meso}^{nj} = characteristic time of mesomixing in nonjet conditions
τ_η = Kolmogorov time scale
τ_A = characteristic time of aggregation
τ_{DS} = characteristic time of diffusion across a shrinking slab
$\tau_{DS,s}$ = characteristic time of diffusion of salt ions across a shrinking slab
$\tau_{DS,p}$ = characteristic time of diffusion of primary particles across a shrinking slab
τ_G = characteristic time of gelation
τ_M = characteristic time of mixing
τ_ω = characteristic time vortex return to isotropy
ϕ = solid volume fraction in the system
ϕ_F = feed solid volume fraction

Literature Cited

1. Odian G. *Principles of polymerization.* 4th ed. Hoboken, NJ: Wiley-Interscience; 2004.
2. Gilbert RG. *Emulsion polymerization: a mechanistic approach.* London: Academic Press; 1995.
3. Russel WB, Saville DA, Schowalter WR. *Colloidal dispersions.* Cambridge: Cambridge University Press; 1989.
4. Delichatsios MA, Probstein RF. Coagulation in Turbulent-Flow—Theory and Experiment. *J of Colloid and Interface Sci.* 1975;51:394–405.
5. Flesch JC, Spicer PT, Pratsinis SE. Laminar and turbulent shear-induced flocculation of fractal aggregate. *AIChE J.* 1999;45:1114–1124.
6. Higashitani K, Yamauchi K, Matsuno Y, Hosokawa G. Turbulent coagulation of particles dispersed in a viscous fluid. *J of Chem Eng of J.* 1983;16:299–304.
7. Kusters KA, Wijers JG, Thoenes D. Aggregation kinetics of small particles in agitated vessels. *Chem Eng Sci.* 1997;52:107–121.
8. Lu CF, Spielman LA. Kinetics of floc breakage and aggregation in agitated liquid suspensions. *J of Colloid and Interface Sci.* 1985;103:95–105.
9. Oles V. Shear-induced aggregation and breakup of polystyrene latex-particles. *J of Colloid and Interface Sci.* 1992;154:351–358.
10. Selomulya C, Amal R, Bushell G, Waite TD. Evidence of shear rate dependence on restructuring and breakup of latex aggregates. *J of Colloid and Interface Sci.* 2001;236:67–77.
11. Serra T, Casamitjana X. Structure of the aggregates during the process of aggregation and breakup under a sheer flow. *J of Colloid and Interface Sci.* 1998;206:505–511.
12. Spicer PT, Keller W, Pratsinis SE. The effect of impeller type on floc size and structure during shear-induced flocculation. *J of Colloid and Interface Sci.* 1996;184:112–122.
13. Smoluchowski M. Versuch einer mathematischen Theorie der Koagulationskinetik kolloider Lösungen. *Zeitschrift für Physikalische Chemie.* 1917;92:129.
14. Melis S, Verduyn M, Storti G, Morbidelli M, Baldyga J. Effect of fluid motion on the aggregation of small particles subject to interaction forces. *AIChE J.* 1999;45:1383–1393.
15. Saffman PG, Turner JS. On the collision of drops in turbulent clouds. *J of Fluid Mechanics.* 1956;1:16–30.
16. Lin MY, Lindsay HM, Weitz DA, Klein R, Ball RC, Meakin P. Universal Diffusion-Limited Colloid Aggregation. *J of Physics-Condensed Matter.* 1990;2:3093–3113.
17. Sandkühler P, Šefčík J, Morbidelli M. Kinetics of gel formation in dilute dispersions with strong attractive particle interactions. *Advances in Colloid and Interface Sci.* 2004;108–09:133–143.
18. Fox RO. *Computational models for turbulent reacting flows.* Cambridge: Cambridge University Press; 2003.
19. Bourne JR. Mixing and the selectivity of chemical reactions. *Organic Process Res & Develop.* 2003;7:471–508.
20. Sparks RG, Dobbs CL. The use of laser backscatter instrumentation for the online measurement of the particle-size distribution of emulsion. *Particle & Particle Systems Characterization.* 1993;10:279–289.
21. Sparks RG, Dobbs CL. The use of laser backscatter instrumentation for the online measurement of the particle-size distribution of emulsions. Vol 10, Pg 279; 1993. *Particle & Particle Systems Characterization.* 1994;11:404–404.
22. Vaccaro A, Šefčík J, Morbidelli M. Modeling Focused Beam Reflectance Measurement and its Application to Sizing of Particles of Variable Shape. Submitted to *Particle & Particle Systems Characterization.* 2005.
23. Bouyer D, Line A, Do-Quang Z. Experimental analysis of floc size

distribution under different hydrodynamics in a mixing tank. *AIChE J.* 2004;50:2064–2081.
24. Baldyga J, Bourne JR. *Turbulent mixing and chemical reactions.* Chichester: Wiley; 1999.
25. Baldyga J, Bourne JR. A fluid mechanical approach to turbulent mixing and chemical reaction: Part II; Micromixing in the light of turbulence theory. *Chem Eng Commun.* 1984;28:243–258.
26. Baldyga J, Bourne JR, Hearn SJ. Interaction between chemical reactions and mixing on various scales. *Chem Eng Sci.* 1997;52:457–466.
27. Baldyga J, Bourne JR, Dubuis B, Etchells AW, Gholap RV, Zimmermann B. Jet reactor scale-up for mixing-controlled reactions. *Chem Eng Res & Design.* 1995;73:497–502.
28. Baldyga J, Bourne JR. A fluid mechanical approach to turbulent mixing and chemical reaction: Part I. Inadequacies of available methods. *Chem Eng Commun.* 1984;28:231–241.
29. Baldyga J, Bourne JR. A fluid mechanical approach to turbulent mixing and chemical reaction. Part III: Computational and experimental results for the new micromixing model. *Chem Eng Communications.* 1984;28:259–281.
30. Baldyga J, Bourne JR. Simplification of micromixing calculations. 1. Derivation and application of new model. *Chem Eng J Biochem Eng J.* 1989;42:83–92.
31. Kusters KA. *The Influence of Turbulence on Aggregation of Small Particles in Agitated Vessels.* Heindoven University of Technology; 1991. PhD Thesis.
32. Luo H, Svendsen HF. Theoretical model for drop and bubble breakup in turbulent dispersion. *AIChE J.* 1996;42:1225–1233.
33. Campolo M, Sbrizzai F, Soldati A. Time-dependent flow structures and Lagrangian mixing in Rushton-impeller baffled-tank reactor. *Chemical Eng Sci.* 2003;58:1615–1629.
34. Deen NG, Solberg T, Hjertager BH. Flow generated by an aerated Rushton impeller: Two-phase PIV experiments and numerical simulations. *Canadian J Chem Eng.* 2002;80:638–652.

Appendix

In order to estimate the values of turbulent energy dissipation rate computation fluid dynamics (CFD) simulations were performed. In our simulations the standard $k - \varepsilon$ model of turbulence was used.[33,34] This model was combined with standard wall function to resolve the near-wall region. The viscosity was set to that of water at 25°C. In order to sufficiently resolve the flow inside the vessel a mesh composed of circa 350,000 cells with particular attention to intense shear and mixing regions was used. For that purpose several refining steps of the mesh near the important regions (impeller and feeding pipe) were performed, which leads to a cell size of around 200 μm in this regions. This size was at least one order of magnitude smaller then the integral scale of turbulence.[24] The value of the turbulent kinetic energy used for estimating the aggregation kernel, the Kolmogorov microscale, as well as the mesomixing time scale was based on the ε value in the fluid volume which lies in the region approximately one pipe diameter away from its end. The estimated value of the Kolmogorov microscale η at a stirring speed $S = 165$ rpm was: $\eta \simeq 50$ μm. Since the presence of the aggregates could have a significant effect on the fluid flow and, consequently, on the turbulent energy dissipation rate, we performed also simulations, where the viscosity was increased 10 times above the original value. The obtained values of the Kolmogorov microscales were approximately 4–5 times larger than those obtained for the original viscosity of water at 25°C. On the other hand, the turbulent energy dissipation rate increases by about 50% of the value calculated for the case with water at 25°C.

Manuscript received May 6, 2005, and revision received Oct. 11, 2005, and final revision received Feb. 27, 2006.